Nanoscale Advances

ROYAL SOCIETY OF CHEMISTRY

PAPER

View Article Online
View Journal | View Issue

Cite this: *Nanoscale Adv.*, 2024, **6**, 1535

p-Phenylenediamine-derived carbon nanodots for probing solvent interactions†

Nidhisha V.,[a] Ritu Gopal,[a] Anjali C.,[a] Amrutha T. P.,[a] Arunima K. K.,[a] Vakayil K. Praveen [bc] and Renuka Neeroli Kizhakayil *[a]

Carbon nanodots, the luminescent nanoparticles of carbon with size restriction below 10 nm, have attracted inordinate attention in materials science due to their widespread applications in optoelectronic and biological fields. Low toxicity and facile synthesis pathways render them favourites in the above-mentioned areas in the context of green chemistry. This work presents fine applications of *p*-phenylenediamine-derived carbon nanodots (PD-CNDs) achieved *via* a facile one-pot hydrothermal method. Adequate characterization using X-ray diffraction and spectroscopic and microscopic studies confirmed spherical particles with an average particle size of 2.8 nm, functionalised with amino, carboxyl, and hydroxyl groups. The carbon framework was functionalised with pyridinic and pyrrolic nitrogens. Upon 365 nm UV light illumination, an aqueous dispersion of PD-CNDs showed red-orange fluorescence. Detailed spectral analysis using UV-visible absorption and fluorescence spectroscopy identified edge states and surface groups as luminescent centres, with a significant contribution arising from the latter. The investigation conducted using a collection of solvents, categorized into polar and nonpolar, indicated the potential of the system for applications based on its solvatochromic nature. The feature enabled the determination of different polarity parameters of the solvents, as well as dielectric constants of solvents and solvent mixtures, with considerable accuracy. The system was potent for predicting the composition of a given pair of solvents. The service of the system is also extended for moisture sensing in organic solvents within an error percentage < 1. High quantum yield values (0.61) combined with solvent composition-dependent optical features ensure broader applications of the system to probe solvent interactions.

Received 20th September 2023
Accepted 2nd February 2024

DOI: 10.1039/d3na00799e

rsc.li/nanoscale-advances

1. Introduction

Since ancient times, carbon has always been a fascinating material that has found numerous fine applications. Tailored carbon materials with excellent physicochemical properties have been designed for highly specialized applications in biological,[1] environmental,[2,3] electronic and catalytic[4,5] fields. It is well known that the applications of materials are manifolded upon reducing the dimensions to nanoframes.[6,7] Nanoconfinement and appropriate functionalization have bestowed additional luminescent features on carbon, which also extends the role of carbon into the optoelectronic field. Carbon nanotubes,[8] nanowires,[9] graphene[10,11] and fullerene[12] fall under this category. Carbon nanodots (CNDs), a comparatively new addition to this family,[13–15] are distinguished for their inherent luminescent feature, which is often excitation dependent. Low toxicity, environmental friendliness, aqueous solubility and resistance to photobleaching render them attractive alternatives to fluorescent dyes and heavy metal-based quantum dots in bioimaging, sensing, catalysis, solar cells and light-emitting diodes. Greener synthesis methods are added advantages for these particles. Herein, we present fluorescence-based fine applications of *p*-phenylenediamine-derived carbon nanodots (PD-CNDs), which are synthesised using a facile one pot hydrothermal method. The system exhibits solvent relaxation/solvatochromism,[16] by virtue of which a material exhibits different colours in different solvents, which is manifested as a change in either the absorption or emission wavelength. Autoclave-based hydrothermal procedures have been widely used to obtain luminescent carbon particles from phenylenediamine systems.[10,17] Solvothermal methods using alcohols, particularly ethanol, have also been reported. Isomer variation has led to CNDs differing in emission wavelength under solvothermal conditions, as shown by Jiang and coworkers.[18] PD-based CNDs have also been established to be fine candidates

[a]*Advanced Materials Research Centre, Department of Chemistry, University of Calicut, Kerala 673635, India. E-mail: renuka@uoc.ac.in*

[b]*Photosciences and Photonics Section, Chemical Sciences and Technology Division, CSIR-National Institute for Interdisciplinary Science and Technology (CSIR-NIIST), Thiruvananthapuram, Kerala 695019, India*

[c]*Academy of Scientific and Innovative Research (AcSIR), Ghaziabad 201002, India*

† Electronic supplementary information (ESI) available: List of selected solvents/solvent mixtures and spectral details. See DOI: https://doi.org/10.1039/d3na00799e

as optical sensors for numerous significant analytes, including metal ions and pH.[19–21] Recently, researchers have begun to explore the solvent effects on these particles by functionalizing the particles with heteroatom containing organic molecules and various polymers[22] as well as long chain aliphatic acids/substituted acids.[23,24]

In the present study, thirteen solvents categorized into polar and non-polar are examined, where the emission wavelength varied almost in the entire VIBGYOR region, depending on the solvent polarity. A detailed investigation supported by spectral data reveals that the photoluminescence of the system originates from edge group/midlevel and surface functional group participation. The system could predict the solvent parameters, such as dielectric constant (ε) and Reichardt's empirical $E_T(30)$ polarity parameter, based on the molar transition energies (E_T) of the Betaine 30 dye in the solvents. Another noteworthy application is the accurate determination of the dielectric constant and composition of solvent mixtures, as exemplified by applying a methanol-1,4-dioxane system. Apart from these, the application is further extended for tracing moisture content in dioxane, which is a commercially significant achievement. An error percentage < 1 assures the proven potential of the system for the above-mentioned applications. The composition-directed emission wavelength noted for the system warrants the extended utility of the system in studying solvent interactions.

2. Experimental section

2.1. Materials

p-Phenylenediamine was purchased from TCI Chemicals (India) Pvt. Ltd. Xylene, toluene, chloroform, dichloromethane, 1,4-dioxane, acetone and silica gel were purchased from SISCO Research Laboratories Pvt. Ltd., India. Methanol and ethanol were purchased from Qualigens Pvt. Ltd. Benzene, 1-butanol, 2-propanol, DMSO, and DMF were obtained from Merck Life Science Pvt. Ltd. MWCO = 1 kDa dialysis membrane (HiMedia) was used as received. All commercially available reagent grade chemicals were used as received without further purification. Deionized (DI) water (resistivity ≈ 18 MΩ), determined using broadband dielectric measurements (Novocontrol broadband dielectric spectrometer in the frequency range of 10^{-2} to 10^{7} Hz) was used for all the experiments reported.

2.2. Synthesis of PD-CNDs

Typically, 50 mg *p*-phenylenediamine was dissolved in 60 mL DI water. The solution was sonicated for 10 min, immediately transferred into a Teflon-lined autoclave, and subjected to hydrothermal treatment for 8 h at 180 °C. After cooling, the aqueous solution was centrifuged at 3000 rpm for 30 min. The filtrate (8 mL) was dialyzed against DI water through a dialysis tube (1 kDa, molecular weight cutoff) for 24 h with a stirring speed of 80 rpm. The final product was vacuum dried and further purified by silica gel (60–120 mesh) column chromatography using 3% methanol–dichloromethane, as the eluent. A fraction with significant luminescence was collected. After the solvent was removed, the residue was dried in a hot air oven at 50 °C for 24 h. The obtained black powder was used for further characterizations and experiments. The schematic of the synthesis procedure is provided in the ESI (Fig. S1, ESI†).

2.3. Characterizations

The morphology of the PD-CNDs was determined using a JEOL JEM 2100 transmission electron microscopy (TEM) instrument, operating at an accelerating voltage of 200 kV. The TEM image-based particle distribution was determined using Image J software. A Rigaku Miniflex-II diffractometer with Cu K_α radiation was used to record the X-ray diffraction (XRD) pattern of the sample in the scan range of 2θ 10−90°. The Raman spectrum was captured using WITec alpha300RRA (WI Tec GmbH, Ulm, Germany) with a 532 nm DPSS laser. Surface element composition was obtained by X-ray photoelectron spectroscopy (XPS) data, which were collected using an Omicron spectrometer with 1253 eV Mg K_α radiation. Zeta potential analysis was carried out using Zetasizer Nano S from Malvern Instruments at 25 °C, and an average of three measurements was taken. The Fourier-transmission infrared (FT-IR) spectrum was recorded using a JASCO FTIR-4700 spectrometer with a smart orbit ATR accessory. UV-vis absorption spectra were recorded using a JASCO V-550 spectrometer. An F-Cary Eclipse fluorescence spectrometer (Aligent Technology) was used to obtain fluorescence spectra. An LZC-4X photoreactor was used to monitor the luminescent features of the systems under UV illumination. Fluorescence lifetime studies were performed using the HORIBA-time correlated single photon counting (TCSPC) system with a 370 nm nanoLED as the excitation source. The photostability of the material was assessed by applying an LZC-4X photoreactor and an F-Cary Eclipse fluorescence spectrometer (Aligent Technology).

2.4. Evaluation of the solvatochromic properties of PD-CNDs

To study the solvatochromic properties of PD-CNDs, their dispersions were prepared at a concentration of 0.1 mg mL^{-1} in solvents with different polarities by sonication for 10 min. The colour changes in day light and UV light (365 nm) were noted. The absorbance and fluorescence spectra of each solution were measured and analysed thereafter.

2.5. Determination of dielectric constant of primary alcohols and alcohol–dioxane mixture

Primary alcohols and mixtures of alcohol and 1,4-dioxane with different ratios (0 to 100%, v/v, with an increment of 10%) were prepared. To this, 0.05 mg mL^{-1} of powdered PD-CNDs was added and dispersed by sonication. The shift in the emission peak maximum of CNDs in various alcohols and alcohol–1,4-dioxane mixtures was monitored using fluorescence spectroscopy.

2.6. Determination of moisture content in 1,4-dioxane

For this purpose, different compositions (0–8% v/v with an interval of 2, and 10–100% v/v with an interval of 10) of 1,4-

dioxane–water mixtures were prepared, and 0.05 mg mL^{-1} of PD-CNDs was added to 10 mL of each of these mixtures and sonicated for 10 min. The fluorescence spectra of these samples were recorded.

3. Results and discussion

3.1. Structural characterization of PD-CNDs

A detailed study on the structure of PD-CNDs is conducted using TEM, powder XRD, FT-IR and Raman spectroscopy. Fig. 1a and b show the TEM images of the particles of <10 nm size. TEM image at higher magnification validated lattice fringes with a *d*-spacing value of 0.19 nm, corresponding to carbon (Fig. 1b inset). Further, the average particle size was determined to be 2.8 nm from the TEM image, as evident from the distribution histogram shown in Fig. 1c.

The powder XRD pattern identifies the extent of crystallinity of the PD-CNDs. The broad peak in the XRD pattern (Fig. 1d) reveals the considerable amorphous nature of the material. The peak at $2\theta = 23.4°$ corresponds to the (002) plane of graphitic carbon.[25] Diffraction peak corresponding to the (100) plane, for which $2\theta \approx 42.4°$, determines the longitudinal dimension of the structural elements.[26] The peak observed at $2\theta = 60°$ corresponds to the (103) plane of carbon in the hexagonal graphitic lattice.[27] Raman spectroscopy gave further information on the nature of the carbon core. In the peak-fitted Raman spectrum depicted in Fig. 1e, both the D and G bands are noted, corresponding to the sp^2 and sp^3 hybrid natures of the carbon atoms, respectively. The in-plane vibrations of sp^2-bonded carbon atoms generate the G band at 1545 cm^{-1}, while the one observed at 1368 cm^{-1} (D band) indicates structural defects in the graphite structure owing to substituted framework carbons, as indicated by the out-of-plane C–C vibrations.[28] The intensity ratio I_D/I_G is found to be 0.88, showing substantial functionalization of the carbon framework in PD-CNDs.[29]

FT-IR spectroscopy and XPS analysis were used to identify the elements and functional groups present in the newly synthesized PD-CNDs. The band appearing at 3427 cm^{-1} in the FT-IR spectrum (Fig. 1f) signifies the –O–H and/or –N–H stretches. The –C=O/–C=N and –C–O stretching generates bands at 1634 and 1121 cm^{-1}, respectively.[30,31] The presence of –C=C and –C–N moieties of the aromatic ring leads to FT-IR bands at 1510 and 1387 cm^{-1}, respectively. Consolidating these data, amino (–NH, $–NH_2$), carbonyl, carboxyl (–C=O/–COOH) and hydroxyl (–OH) functionalized carbon cores are visualized in PD-CNDs. More precise information on the structure is collected from the XPS results. Three major peaks are identified in PD-CNDs at 288.75, 402.51 and 534.75 eV, which are attributed to C 1s, N 1s and O 1s (Fig. 2a) with corresponding atomic percentages of 71.88, 11.41, and 14.71%, respectively. The peaks obtained are carbon corrected by 4.2 eV. Fig. 2b displays that the C 1s peak was further fitted to mark the moieties C–C/C=C (284.35 eV), C–N/C–O (285.31 eV), and C=N/C=O (286.36 eV).[30] Prediction on the nature of nitrogen linkage is made easy by curve fitting the N 1s spectral peak, which is composed of three peaks, pyridinic, pyrrolic and amino N's, at 398.39, 400.18 and 399.21 eV, respectively (Fig. 2c).[32] The presence of nitrogen in the framework and amino functionality is thus quite evident.

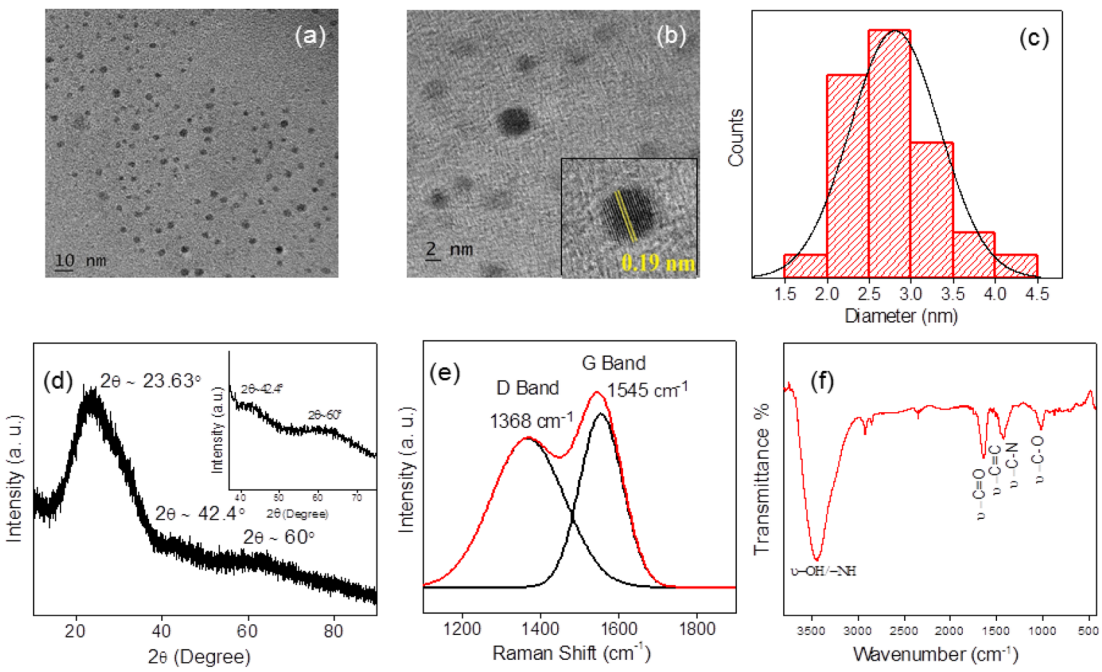

Fig. 1 (a) and (b) TEM images of PD-CNDs at different magnification levels, inset of Fig. 1b shows the lattice fringes with *d*-spacing value of 0.19 nm. (c) Particle size distribution determined from the TEM, (d) powder XRD profile, (e) curve fitted Raman spectrum and (f) FT-IR spectrum of PD-CNDs.

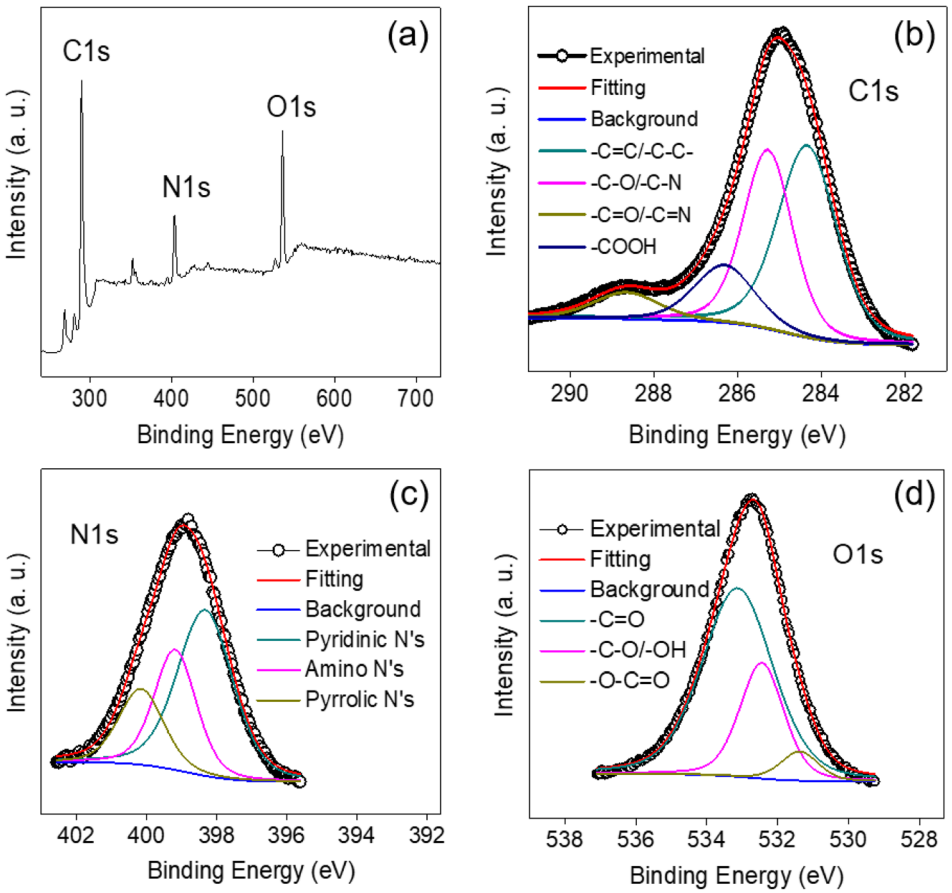

Fig. 2 (a) XPS survey spectrum of PD-CNDs, (b)-(d) XPS fitting curves of C 1s, N 1s and O 1s of PD-CNDs, respectively.

The O 1s peak upon curve fitting shows the presence of functionalities, C═O, C–O/C–OH and O–C═O, as indicated by peaks at 531.37, 532.47 and 533.14 eV in the respective order (Fig. 2d).[33] Combining the XPS and FT-IR details, a carbon core rich with amine groups, carboxyl moieties and hydroxyl groups is envisaged in PD-CNDs, the carbon framework of which includes pyridinic and pyrrolic nitrogens.

3.2. Solvent-induced optical features of PD-CNDs

In the solid state, PD-CNDs prepared *via* hydrothermal treatment were non-luminescent under UV irradiation. However, solvent-induced luminescence was exhibited by them. The images of aqueous dispersions of PD-CNDs in day light and UV light are shown in Fig. 3a. Aqueous dispersion that appeared brownish red in visible light emitted a reddish orange colour under UV illumination (365 nm). The luminescence in carbon particles results from the recombination of photoinduced charge carriers originated either from the core or surface functional groups. The edge states bordering the core also generate these exciton pairs.

A detailed investigation of the solvent-induced optical properties of the system is conducted using UV-Vis absorption and photoluminescence spectroscopy. Fig. 3b shows the UV-Vis absorption spectrum of *p*-phenylenediamine-derived CNDs. The absorption consists of a broad spectrum extending to the visible range. Prominent peaks are observed at 278 nm in the high-energy UV range, and 510 nm in the visible region. Apart from these, one shoulder peak was also noted at around 365 nm. The peaks noted in the 240–280 nm region are assigned to π–π* transition of carbonyl, aromatic C═C double bond and –C═N groups. The shoulder peak at ~365 nm accounts for n–π* transition arising from various surface functional groups.[34,35] Extended π-conjugation in the carbon structure leads to a peak at 510 nm and explains the Mie scattering.[36]

The photoluminescence spectrum of the PD-CNDs is displayed in Fig. 3c. It is clear from the spectrum that the system is a dual emissive with two emission maxima at 504 and 618 nm; the net emission is reddish orange under UV illumination (Fig. 3a). Analysis of the excitation dependency nature (Fig. 3d) reveals that the emission peak at 504 nm is excitation wavelength dependent in nature, while the position of the second emission peak at 618 nm is unaltered. This is typically due to the presence of different emissive states on CNDs and is attributable to functional groups in the structure. The peak at the lower wavelength shows a red-shift and vanishes slowly with an increase in excitation wavelength. As per previous reports, this shift can be attributed to surface defect emission.[37] Luminescence-based fine applications mandate the photostability of the fluorophore species. Thus, the photostability of

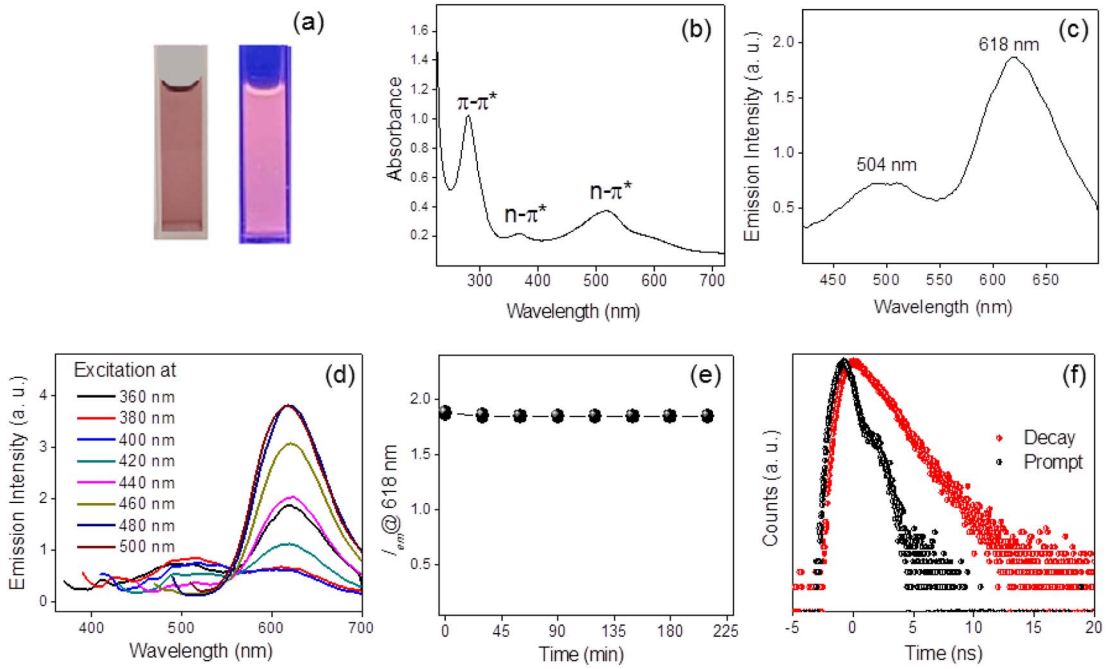

Fig. 3 (a) Aqueous dispersion of the PD-CNDs under day light and 365 nm UV light, (b) UV-vis absorption spectrum, (c) fluorescence emission spectrum of PD-CNDs (λ_{ex} = 360 nm), (d) excitation dependent emission behavior of PD-CNDs, (e) photostability curve, and (f) fluorescence lifetime decay profile of PD-CNDs (λ_{em} = 618 nm) (red circles). Instrument response function (prompt) is obtained at 368 nm (excitation wavelength) using milk powder suspension (black circles).

CNDs was checked by the continuous exposure of the solution to UV radiation, and the data presented in Fig. 3e show that the emission intensity (λ_{max} = 618 nm) of these particles is significantly stable when dispersed in aqueous medium. The quantum yield of PD-CNDs determined using Rhodamine B in water as the reference was 0.61. The fluorescence lifetime profile of the CND dispersion monitored at 618 nm was best fitted with a mono-exponential decay with a time constant of 2.40 ns (Fig. 3f). The surface charge of PD-CNDs were analysed in water using zeta potential measurements and was found to be positive (55 mV), indicating good dispersion stability of the nanomaterial[38] (Fig. S2, ESI†).

3.2.1. Solvatochromism in PD-CNDs. An in-depth analysis of the solvent-induced luminescence character of PD-CNDs is carried out using solvents of different polarity, including benzene, toluene, xylene, chloroform, dichloromethane, DMSO, ethanol, methanol, 1-butanol, isopropyl alcohol (IPA), DMF, acetone and water. Their characteristics, including dielectric constant and $E_T(30)$ relative polarity, are listed in Table 1. The photographs of dispersion of PD-CNDs (0.1 mg

Table 1 Solvent polarity parameters of solvents selected for the study and fluorescence emission peak maximum, λ_{max} (em) of PD-CNDs in these solvents

Sl. No.	Solvent	Type	Dielectric constant (ε)	Relative polarity	$E_T(30)$	Kamlet Taft parameters			λ_{max} (em) nm
						α	β	π^*	
1	Toluene	Nonpolar	2.38	0.099	33.9	0	0.11	0.54	532.76
2	Benzene	Nonpolar	2.28	0.111	34.5	0	0.10	0.59	529.55
3	Xylene	Nonpolar	2.37	0.074	33.3	0	0	0.47	530.54
4	Dichloromethane	Polar aprotic	8.93	0.309	41.1	0.13	0.10	0.82	537.66
5	Chloroform	Polar aprotic	4.81	0.259	39.1	0.44	0	0.58	535.00
6	Acetone	Polar aprotic	20.7	0.355	42.2	0.08	0.43	0.71	555.00
7	DMF	Polar aprotic	36.7	0.386	43.8	0	0.69	0.88	571.64
8	DMSO	Polar aprotic	47.0	0.444	45.0	0	0.76	1.00	579.87
9	1-Butanol	Polar protic	17.8	0.586	50.2	0.79	0.88	0.47	593.00
10	Isopropyl alcohol	Polar protic	18.3	0.546	48.6	0.8	0.5	0.5	586.60
11	Ethanol	Polar protic	24.6	0.654	51.9	0.86	0.75	0.54	596.50
12	Methanol	Polar protic	32.6	0.762	55.5	0.98	0.66	0.60	605.53
13	Water	Polar protic	78.54	1.000	63.1	1.17	0.47	1.09	618.01

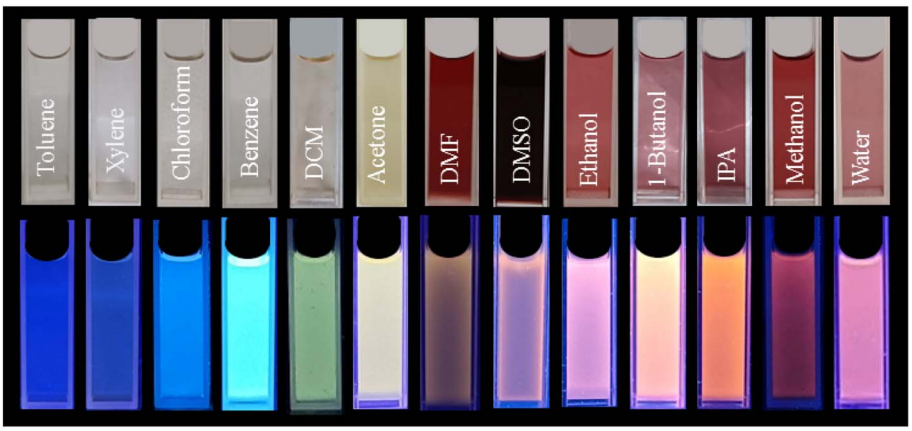

Fig. 4 Photographs of dispersion of PD-CNDs in selected solvents. Upper panel under day light and lower panel under 365 nm UV illumination.

mL^{-1}) in various solvents are shown in Fig. 4, which demonstrates that the system exhibits different colours in different solvents, thus exhibiting "solvatochromism", *i.e.*, "change in colour due to solvent effects". The property is maintained in all the thirteen solvents tested and is visible both under day light and UV light, indicating that both the ground and excited states of the PD-CNDs are influenced by the polarity of the solvents. Quite interestingly, the luminescence of the system spreads almost throughout the entire VIBGYOR region.

Analysis of the absorption spectral features provides information on solute–solvent interactions, as indicated by the absorption maximum wavelength. The categorization of the solvents based on polarity is attempted for a fair comparison of the data. The absorption spectrum of PD-CNDs recorded in these selected solvents (Fig. 5a and b) indicates that the intensity, shape, and position of the absorption peaks of PD-CNDs differ significantly with the nature of the solvents. The wavelength corresponding to the absorption maxima increased sequentially for protic solvents. But this is not much pronounced in the case of aprotic solvents. Intermolecular solute–solvent interactions (such as H-bonding, dipole–induced dipoles, dipole–dipole and ion–dipoles), which primarily affect the ground and excited state energy difference of the species, are instrumental for these variations.

Fig. 5a represents the UV-Vis absorption spectra of PD-CNDs in nonpolar solvents, in which they could be dispersed to a certain extent, showing π–π* and n–π* transitions. The nonpolar solvents can interact with CNDs *via* dipole–dipole interaction, which leads to stabilization of the ground state of the PD-CNDs, thereby causing a small hypsochromic shift in the π–π* transition peak in these solvents.[39] Fig. 5b shows the absorption spectra of CNDs in polar solvents, and the inset highlights the absorption spectra in the visible region. A pronounced shift in the absorbance maxima is obvious from Fig. 5, indicating that the interaction of PD-CNDs with solvents differs widely. The influence of solvent polarity on absorbance, especially in H-bonding (HB) solvents, is attributed to the n–π* transition occurring from the edge atom into π* orbital of the core. This movement of charges induces a change in dipole

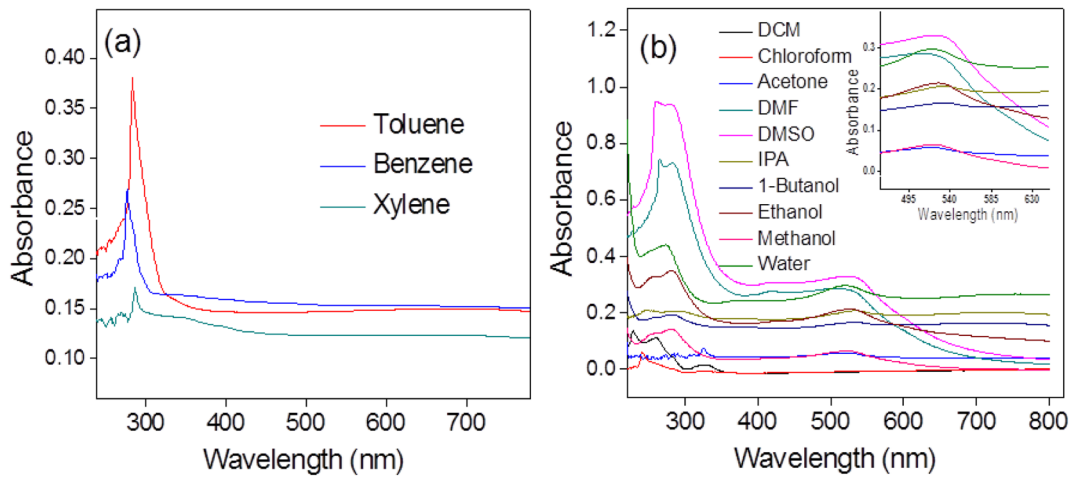

Fig. 5 (a) UV-vis absorption spectra of PD-CNDs dispersion in nonpolar solvents and (b) in polar solvents. The inset in (b) corresponds to absorption spectra in the visible region.

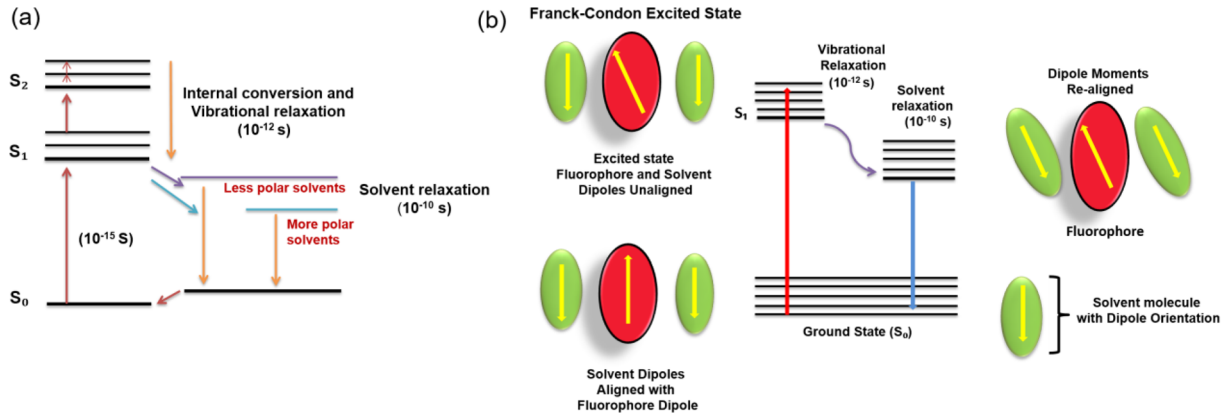

Fig. 6 (a) Jablonski diagram for fluorescence with solvent relaxation and (b) fluorophore-solvent excited state interaction.

moment favouring the absorption of energy corresponding to this.[40]

The fluorescence solvatochromism is caused by dipole interactions between the solvent molecules and the CND surface. The dipole moment substantially affects the electrical structure of the surface as the solvent polarity increases. It also shrinks the energy gap, which causes the red-shift of fluorescence emission wavelength. The ground and excited states of the fluorophore have different energies, resulting in a change in the molecular dipole moment, which eventually causes the solvent molecules in the vicinity to rearrange. However, as per the Franck–Condon principle, the time frame for the excitation of the molecule to a higher electronic level is much less when compared to the time taken for the solvent molecules to reorient around the former. The dipole moment of the fluorophore in the excited state is much higher than that in the ground state, which quickly transfers the excess vibrational energy to nearby solvent molecules, as it gradually relaxes to the lowest vibrational energy level (occurring in the picosecond time scale). By slowly rotating (a process known as solvent relaxation) around the excited fluorophore, which takes between 10 and 100 picoseconds, solvent molecules stabilize and lower the energy level of the excited state.

Owing to the reduced energy gap between the ground and excited states, the fluorescence emission is red-shifted (λ_{max} shifted to longer wavelength). The Jablonski diagram for fluorescence with solvent relaxation and fluorophore-solvent excited state interactions is depicted in Fig. 6.

Fig. 7a illustrates the solvent polarity-dependent fluorescence spectra of PD-CNDs at an excitation wavelength of 420 nm. The corresponding normalized spectra of the PD-CNDs in the selected solvents are shown in Fig. 7b. The intensity of emission was found to be weak with solvents of the lowest and highest polarity. In some previous reports, this change was attributed to the reduced dispersibility of carbon particles in these solvents owing to the amphiphilic and polarized surface of carbon particles. The twisted intramolecular charge transfers between the solvent and the carbon particles as well as the proximity effect are also cited as a reason for this.[41,42] In the proximity effect, loss of excitation energy is achieved in a non-radiative manner when fluorophores are in close proximity, where additional non-radiative relaxation pathways are generated with a polarity increase in solvents and contribute more to luminescence reduction. The quantum yield values obtained in the two representative solvents justify this statement. The

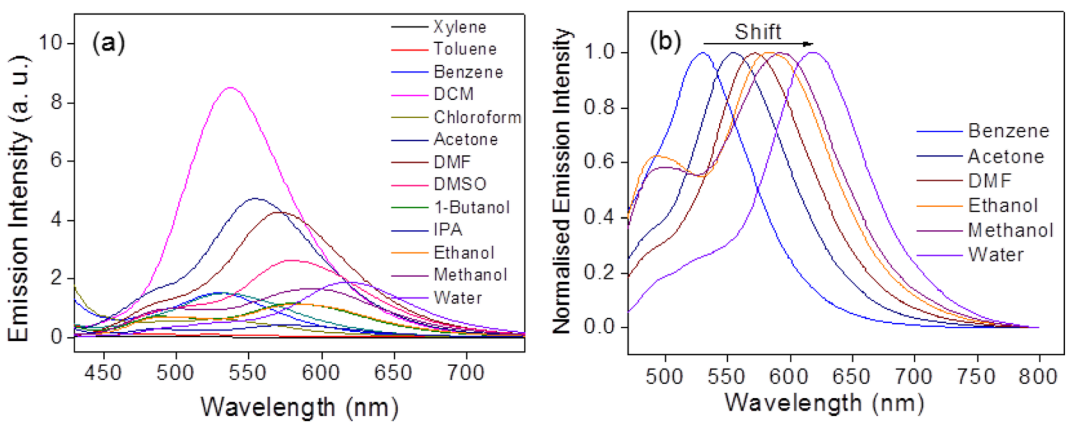

Fig. 7 (a) Solvent polarity dependent fluorescence spectra of PD-CNDs (λ_{ex} = 420 nm) and (b) corresponding normalized fluorescence spectra to explicitly mark the shift in wavelengths with solvent polarity change.

quantum yield values determined in benzene and water are 0.82 and 0.61, respectively. A visible bathochromic shift in fluorescence from blue to red with an increase in the polarity of the medium is evident in the spectra (Fig. 7b). H-bonding-induced emission (HBIE) accounts for the emission features of the system in polar solvents, mediated through H-bonding between the carbon particle surface and H-bond donating (HBD) protic solvents.[43,44]

The fluorescence maxima (λ_{em}) in different solvents are listed in Table 1. As the polarity of the solvent increases, the λ_{em} values are shifted to longer wavelengths. It is noteworthy that the intervals of fluorescence peak positions are closer to each other for aprotic solvents and that the corresponding differences among protic solvents are much higher. The emission peaks are red-shifted by 86 nm when the dispersion medium changed from toluene to water. The fluorescence red-shifts with increasing solvent polarity from toluene (532 nm/2.33 eV) to water (618 nm/2.00 eV), demonstrating a maximum shift of 0.33 eV. The above-mentioned red-shift of emission in protic solvents demonstrates that the H-bonding acceptor character of PD-CNDs is more promoted by photo-excitation, which is attributed to increased negative charge localized in the H-bonding acceptor groups on the carbon surface, an inference supported by UV-Vis absorbance and photoluminescence spectral methods.[45,46] The shift is found to be far higher than those of the other CNDs, showing the solvatochromic behavior.[40]

A characteristic feature noted for the system was the absence of an emission peak at higher energy (lower wavelength region), even when high energy radiation was used for excitation (Fig. S3, ESI†). It is obvious that emissions from the carbon core are expected at higher energies, which is not observed here. With the considerable sp^3 character of the carbon core, the emission from the core can be from isolated sp^2 clusters with a large energy gap attached to the periphery of carbon particles.[47] The HOMO–LUMO π–π^* energy gap of such sp^2 clusters is analogous to the pyridine moieties anchored on the carbon core (3 eV), which is far higher than the emission energy from the surface states.[47,48] Absence of emission peak below 300 nm thus indicates the absence of emission from the core that emits at higher energy, attributed to radiative excitonic recombination across the core band gap. The emission in the 400–500 nm region matches with edge-state excitation, while the emission noted at higher wavelength (≥500 nm) (low energy peak noted in Fig. 3c) originates from surface fluorophores.[16] Compared to surface group participation, edge group emission is significantly low. It is clear from Fig. 7b that PD-CNDs show a shift in the emission maxima upon changing the solvents from toluene to water, typically from nonpolar to polar solvents.

The emission exhibited by the PD-CNDs was excitation wavelength dependent, as shown in Fig. 8. As the excitation wavelength shifts from 360 to 500 nm, there is a clear red-shift for the emission peaks of CNDs in a given solvent. Emission from the species is noted in two regions, namely 400–500 nm

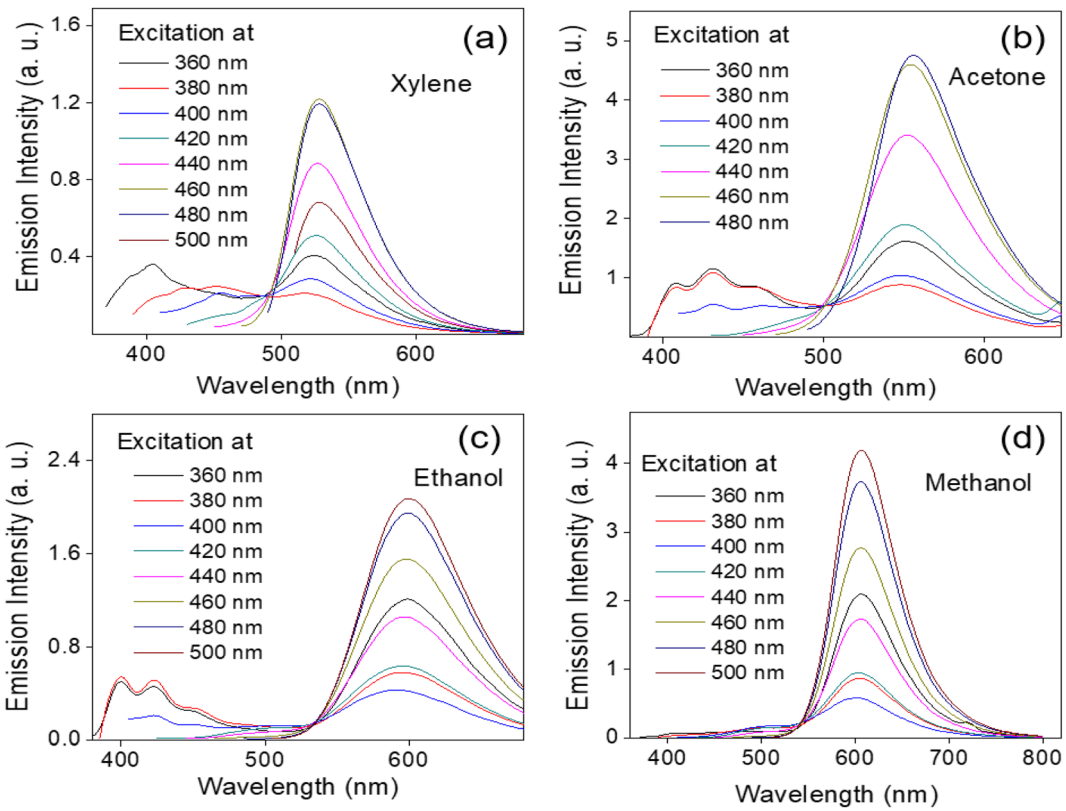

Fig. 8 Fluorescence emission spectra of PD-CND dispersions in (a) xylene, (b) acetone, (c) ethanol and (d) methanol at different excitation levels.

range at λ_{ex} 360 to 420 nm, and at >500 nm, which is invariably fixed whatever the energy of excitation is. This observation was also noted previously in water (Fig. 3c). The dependence on excitation wavelength observed in the edge emission state (from 400 to 500 nm) shows that the fluorescence centres responsible for edge-state emission are distributed in a wide energy range and illustrates the red edge excitation shift. However, in the range of $\lambda_{ex} = 420–500$ nm, the emission spectra were identical, with only one peak at a higher wavelength region (500–620 nm), except that the intensities steadily decreased as the emission energy decreased.

The polarity-dependent solvatochromic character can be explained in terms of a commonly used qualitative solvent polarity parameter, namely $E_T(30)$.[49] The solvent polarity effect on a Betaine dye with respect to the S_0 to S_1 transition was used to model the $E_T(30)$ scale. When the fluorescence and absorption maxima are plotted against the $E_T(30)$ scale, solvatochromic behaviour can be predicted. Fig. 9a shows the plot of the emission maximum (λ_{em}) value *versus* the polarity parameter $E_T(30)$ of the solvents used for dispersing PD-CNDs. The values of $E_T(30)$ for various solvents under investigation, adopted from the literature[49] are listed in Table 1. A fairly good linear relation is shown between the emission maximum wavelength of PD-CNDs and the corresponding $E_T(30)$ values in different solvents. The specific nature of the interactions between the solute and solvents is indicated by the relationship. The linear trend observed in fluorescence indicates that the red-shift in emission is dependent on solvent polarity.[50]

The dielectric constant (ε), which quantifies the polar nature in terms of the amount of electrical energy stored in the electric field of the solvent, constitutes another parameter that best describes solvent polarity. The dielectric constant values of the solvents selected (Table 1) when plotted against their emission maxima (λ_{em}) values are shown in Fig. 9b. Two distinct variations in the parameter are evident from the plot, signifying (i) polar protic solvent and (ii) polar aprotic and nonpolar solvents. This unambiguously proves the influence of H-bonding in determining the emission maximum in different solvents. Indirectly, we can predict the dielectric constant values of solvents from the region. Polar protic solvents can be distinguished from the rest of the solvents from the emission maxima values falling in the range higher than 580 nm. In the case of polar protic solvents, more specific interactions between PD-CNDs and solvent can be identified, an H-bonding interaction highly probable between the alcoholic solvent and oxygen/nitrogen rich functionality in the PD-CNDs.[51]

3.2.2. Solvatochromism-mediated applications of PD-CNDs

3.2.2.1. Determination of dielectric constants of primary alcohols and alcohol–1,4-dioxane mixtures. The sharp change in emission maximum with variation in solvent polarity opens up the scope for analysing the properties of solvent mixtures. As a direct application, this material can be used to give an idea about the dielectric constant values of primary alcohols. Dielectric constants of the materials constitute an important parameter that is decisive in many of the applications.[52–55] Fig. S4, ESI† shows the data in this regard. The corresponding values of physical parameters are depicted in Table S1, ESI.† The linear relationship observed between the emission maxima and dielectric constant values of primary alcohols substantiates this proposal.

The scope of the results is further extended to alcohol–dioxane mixtures. The solvatochromic effect of PD-CNDs is visible in day light and is more pronounced under UV illumination, as shown in Fig. 10, showing the photographs of PD-CND dispersions (0.05 mg mL^{-1}) in mixtures of 1,4-dioxane and methanol with different ratios (0, 10, 20, …, 100%, v/v, with increment of 10%) under day light and 365 nm UV light.

The UV absorbance profiles of these PD-CND dispersions of different compositions of methanol-1,4-dioxane are shown in Fig. S5, ESI.† A significant shift is observed in the n–π* transition with an increase in the methanol content in the mixture. The fluorescence emission spectra of these dispersions excited at the optimum wavelength of 460 nm are presented in Fig. 11a, and the normalized spectra of selected compositions are presented in Fig. 11b. The changes in the emission wavelength and

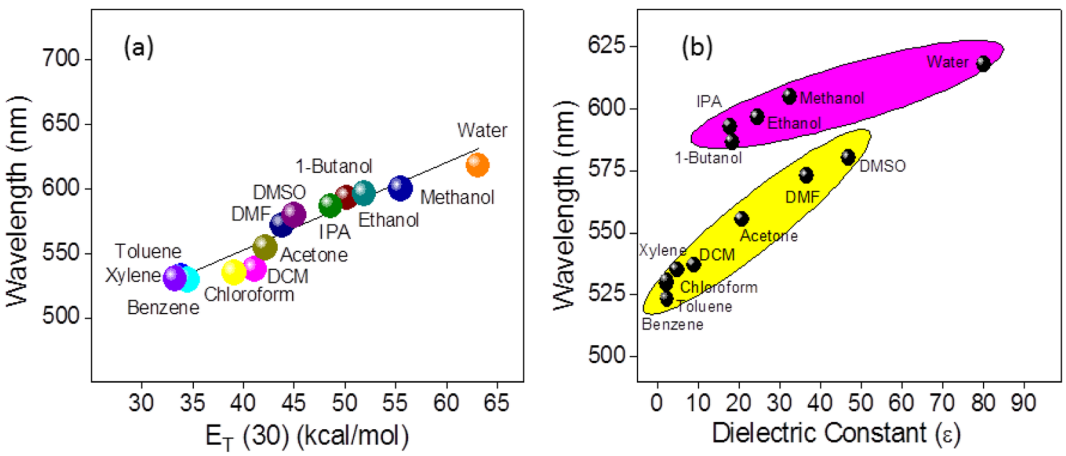

Fig. 9 (a) Plot of fluorescence emission maximum values, λ_{max} (em), of PD-CNDs dispersion in selected solvents *versus* $E_T(30)$ and (b) λ_{max} (em) values *versus* dielectric constant of solvents used for dispersing PD-CNDs.

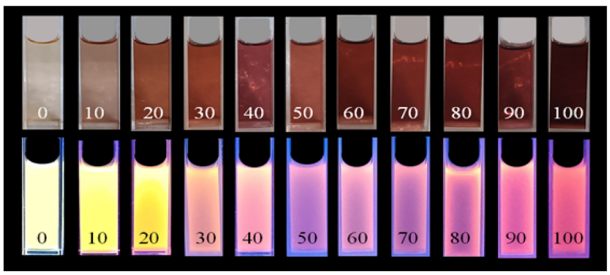

Fig. 10 Photographs of PD-CND dispersions in different compositions of methanol–1,4-dioxane mixture (from 0 to 100%, with 10% increment) in the increasing order of methanol content. Images under day light (upper panel) and under 365 nm UV light illumination (lower panel).

methanol content in the binary mixture are summarised in Fig. 11c. The bathochromic shift of emission maximum varies linearly with methanol content in three ranges: from 0 to 5, 5 to 40 and 40 to 100%. These results demonstrate that quantification of the solvent in the mixture is possible using *p*-phenylenediamine-derived CNDs. Experiments conducted using some mixtures (33 and 52% methanol) confirm the reliability of the results, obtaining 33.03 and 52.09 as the compositions demonstrated in Fig. 11c.

Apart from these, another significant result is also obtained from these data. As the emission feature is related to the polarity of the medium, it is reasonable to expect that the trend in variation in dielectric constant with composition should be reflected in the emission maxima in mixtures, as the polarity of solvents drastically affects the emission features of these particles. The dielectric constants of dioxane–methanol mixtures of varying compositions were reported by Papanastasiou *et al.*, which is used as a reference here.[56] Illustration presented in Fig. 11d shows the validity of this. The same trend is followed for compositions and dielectric constants when plotted against the λ_{max} obtained for various mixtures, which in turn enabled the determination of dielectric constant values of a given methanol–1,4-dioxane mixture. Related parameters are presented in Table S2, ESI.†

3.2.2.2. Determination of moisture content in 1,4-dioxane–water mixtures. Nonpolar solvents are often used as solvents for organic reactions, and water can have an unfavourable impact on various chemical reactions by hindering not only the yield but also the rate of reactions and their applications. This obviously demands a straight forward, fast and trustworthy analytical method for precisely quantifying water in organic solvents for synthetic laboratories and industrial applications. One of the most used techniques for water detection with excellent selectivity and accuracy is the Karl-Fischer titration.[57] Fluorescence-based techniques have been suggested as an alternative to Karl-Fischer titration for determining moisture content owing to their advantages, such as high sensitivity, operational simplicity, rapid response and low cost.[58]

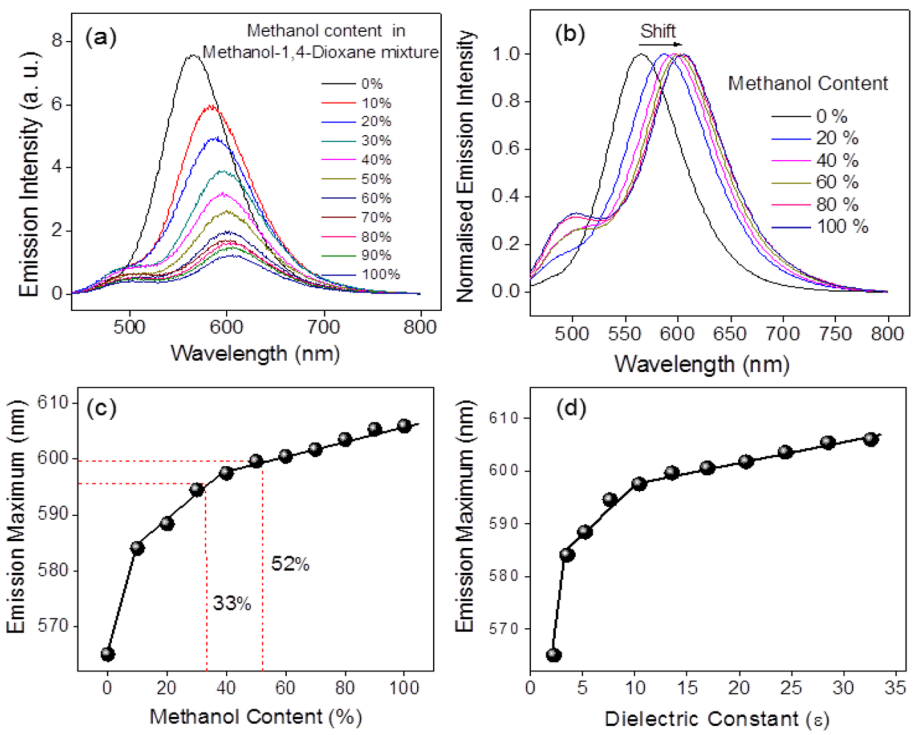

Fig. 11 (a) Fluorescence emission spectra of PD-CNDs at selected compositions (0 to 100% with 10% increment), and (b) normalised emission spectra of PD-CNDs in selected composition of methanol–1,4-dioxane mixture (0, 20, 40, 60, 80 and 100% v/v) ($\lambda_{ex} = 460$ nm). (c) Plot showing the relationship of emission peak maximum *versus* methanol content in the binary mixture and (d) plot of emission peak maximum *versus* dielectric constant.

Herein, a simple and efficient fluorescence-based technique is offered using PD-CNDs to measure the moisture content in 1,4-dioxane. Typically, 0.05 mg of PD-CND powder was dispersed in 10 mL of different compositions of the 1,4-dioxane–water mixture (0 to 100% v/v with an increment of 10%), and changes in the fluorescence wavelengths were noted. Photographs of PD-CND dispersion at these compositions under visible and UV light illumination are shown in Fig. 12. As is obvious, there is a significant difference in the colour of the dispersions both in visible light and under UV light. As the water content increased in 1,4-dioxane, a gradual shift to dark brown colour is noted for the dispersions, which indicates that the absorbance of these systems varies from mixture to mixture. The UV-vis absorbance profiles of the PD-CND dispersions of different compositions (Fig. S6, ESI†) confirm a shift in the n–π* transition of CNDs with an increase in the water content in the mixture. The solvatochromic influence is even more pronounced in the fluorescence images recorded under UV light (365 nm) illumination. A gradual variation in luminescence colour from yellow to pink is clearly observed with an increase in the percentage of water in the PD-CND 1,4-dioxane–water dispersion.

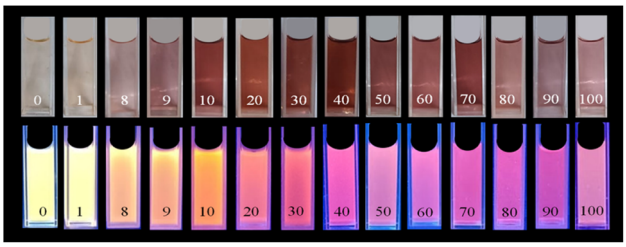

Fig. 12 Photographs of PD-CND dispersions in different compositions of 1,4-dioxane–water mixture (0, 1, 8, 9, 10, and thereafter with an increment of 10% up to 100% v/v) in the increasing order of water content. Images under day light (upper panel); under 365 UV illumination (lower panel).

The fluorescence spectrum of each composition, λ_{ex} = 420 nm (Fig. 13a), indicates a dramatic decrease in the fluorescence intensities of PD-CNDs in 1,4-dioxane with small bathochromic shift upon increase in water content in the mixture (0 to 100%, v/v). The normalized emission spectrum of the system with various compositions displayed in Fig. 13b indicates a drastic variation in emission wavelength due to the presence of very small amounts of water as low as 1%.

As shown in Fig. 13c, the red-shift in emission maximum with increasing water content in 1,4-dioxane traces two linear variations observed in two different ranges, 0–10 and 11–100% of water content, with R^2 values of 0.9673 and 0.9953, respectively. The difference in slope may be because the PD-CNDs are preferentially solvated by relatively less polar 1,4-dioxane in the binary solvent mixtures. The observed bathochromic shift and fluorescence quenching could be attributed to the general solvent effects and the H-bonding interaction of various

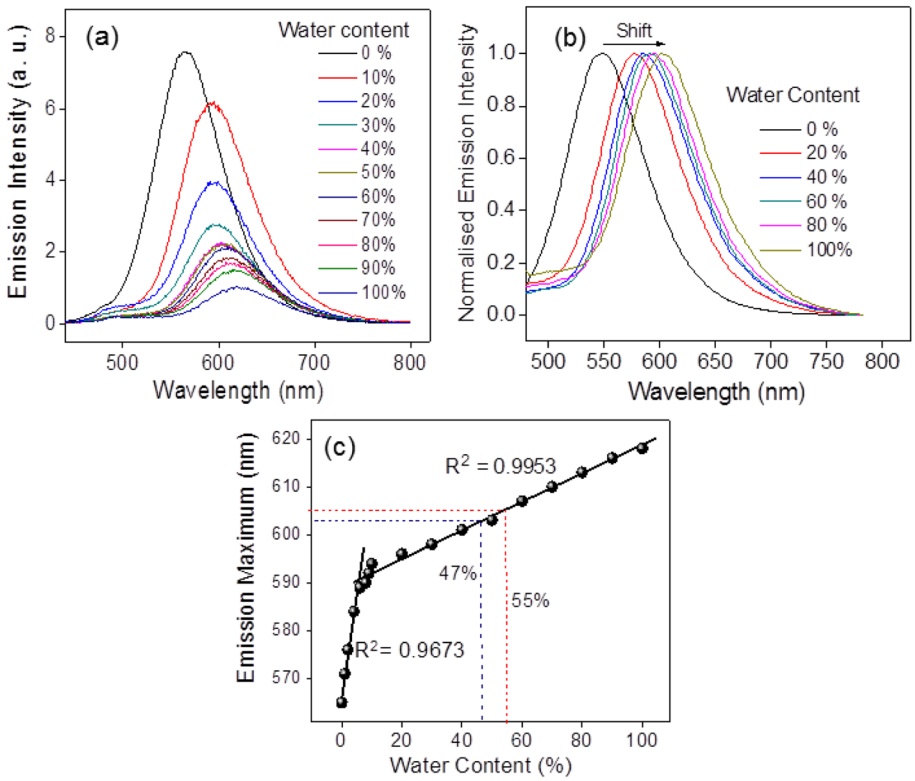

Fig. 13 (a) Fluorescence emission spectra of PD-CNDs in 1,4-dioxane–water composition (0 to 100% with 10% increment) and (b) normalised emission spectra of PD-CNDs in selected 1,4-dioxane–water compositions (0, 20, 40, 60, 80 and 100%, v/v) (λ_{ex} = 420 nm). (c) Plot showing relationship of emission peak maximum *versus* water content in 1,4-dioxane.

functional groups of PD-CNDs with water molecules.[59] Validation of the experiment is done by conducting the spectral study of two mixtures of 1,4-dioxane and water of different compositions, with 47 and 55% of water. The significant reliability of the results is assured from the compositions predicted from the plot, 46.54 and 54.68% in the respective order, with <1% (0.97 and 0.58%, respectively) errors.

Conclusions

In this work, highly luminescent CNDs are synthesised from *p*-phenylenediamine using a straightforward one-step hydrothermal method. The CNDs possess a carbon framework containing pyridinic and pyrrolic nitrogens and amino, carboxyl, and hydroxyl groups as surface functionalities. The CNDs displayed inherent luminescence in red-orange colour. Edge group/midlevel and surface functional group participation were inferred as the origin of luminescence in these particles. One of the key findings of this work is the solvatochromic behaviour of PD-CNDs, wherein they exhibit different photoluminescence colours when dispersed in different solvents. A novel method for predicting solvent polarity parameters is suggested using a system based on the solvatochromic nature. Accurate determination of the dielectric constants of solvents and binary solvent mixture is validated, as exemplified by applying the methanol-1,4-dioxane system. A simple and effective approach is developed for quantitatively determining moisture in organic solvents, with an error percentage below one. The emission colour of the solutions varied with water content in the organic solvent, with a red shift in emission wavelength. Experiments carried out using 1,4-dioxane–water binary mixtures reveal the commendable validity of the procedure. Even naked-eye monitoring of moisture content was possible under 365 UV light illumination. The solvent-dependent emission features of the PD-CNDs open up broader opportunities for the material to study solvent interactions. The low toxicity, facile synthesis and solvent-dependent fluorescence make PD-CNDs promising candidates for a wide range of future scientific and technological area applications.

Conflicts of interest

There are no conflicts to declare.

Acknowledgements

N. V. acknowledges University of Calicut for the research fellowship. The authors are grateful to CSIF-University of Calicut, CIF-IISER-Thiruvananthapuram, STIC-CUSAT for analytical support. V. K. P. is grateful to the Council of Scientific and Industrial Research (CSIR) for providing the infrastructure and research facilities. R. N. K. gratefully acknowledges DST, Government of India, for the research facilities provided under FIST.

References

1 M. Mohajeri, B. Behnam and A. Sahebkar, *J. Cell. Physiol.*, 2019, **234**, 298–319.
2 H. Filik and A. A. Avan, *Arabian J. Chem.*, 2020, **13**, 6092–6105.
3 Y.-n. Zhang, Q. Niu, X. Gu, N. Yang and G. Zhao, *Nanoscale*, 2019, **11**, 11992–12014.
4 P. Serp and B. Machado, *Nanostructured Carbon Materials for Catalysis*, The Royal Society of Chemistry, Cambridge, 2015.
5 L. Wang, Z. Liu and J. Zhang, *Nanoscale*, 2022, **14**, 13473–13489.
6 D.-S. Wang, A. Mukhtar, K.-M. Wu, L. Gu and X. Cao, *Materials*, 2019, **12**, 3908.
7 D. Wang, A. Mukhtar, M. Humayun, K. Wu, Z. Du, S. Wang and Y. Zhang, *Chem. Rec.*, 2022, **22**, e202200016.
8 R. Rao, C. L. Pint, A. E. Islam, R. S. Weatherup, S. Hofmann, E. R. Meshot, F. Wu, C. Zhou, N. Dee and P. B. Amama, *ACS Nano*, 2018, **12**, 11756–11784.
9 A. Hua, Y. Li, D. Pan, J. Luan, Y. Wang, J. He, S. Tang, D. Geng, S. Ma and W. Liu, *Carbon*, 2020, **161**, 252–258.
10 M. J. Allen, V. C. Tung and R. B. Kaner, *Chem. Rev.*, 2010, **110**, 132–145.
11 R. Ye and J. M. Tour, *ACS Nano*, 2019, **13**, 10872–10878.
12 P. Bhakta and B. Barthunia, *J. Indian Acad. Oral Med. Radiol.*, 2020, **32**, 159–163.
13 J. Liu, R. Li and B. Yang, *ACS Cent. Sci.*, 2020, **6**, 2179–2195.
14 V. Ansi, K. Vijisha, K. Muraleedharan and N. K. Renuka, *Sens. Actuators, B*, 2020, **302**, 111817.
15 P. V. Raveendran and N. K. Renuka, *Mater. Chem. Phys.*, 2022, **288**, 126236.
16 N. Basu and D. Mandal, *J. Phys. Chem. C*, 2018, **122**, 18732–18741.
17 H. Li, X. Yan, S. Qiao, G. Lu and X. Su, *ACS Appl. Mater. Interfaces*, 2018, **10**, 7737–7744.
18 K. Jiang, S. Sun, L. Zhang, Y. Lu, A. Wu, C. Cai and H. Lin, *Angew. Chem., Int. Ed.*, 2015, **54**, 5360–5363.
19 Y. Sun, X. Wang, C. Wang, D. Tong, Q. Wu, K. Jiang, Y. Jiang, C. Wang and M. Yang, *Microchim. Acta*, 2018, **185**, 83.
20 C. Tan, X. Su, C. Zhou, B. Wang, Q. Zhan and S. He, *RSC Adv.*, 2017, **7**, 40952–40956.
21 J. Chen, J.-S. Wei, P. Zhang, X.-Q. Niu, W. Zhao, Z.-Y. Zhu, H. Ding and H.-M. Xiong, *ACS Appl. Mater. Interfaces*, 2017, **9**, 18429–18433.
22 H. Ding, S.-B. Yu, J.-S. Wei and H.-M. Xiong, *ACS Nano*, 2016, **10**, 484–491.
23 K. Sato, R. Sato, Y. Iso and T. Isobe, *Chem. Commun.*, 2020, **56**, 2174–2177.
24 J. Bai, G. Yuan, Y. Zhu, Z. Huang, L. Zhang, X. Wang, S. Wu and L. Ren, *J. Phys. Chem. C*, 2021, **125**, 18543–18551.
25 V. A. Ansi, P. Thasleena, A. A. Anappara and N. K. Renuka, *Int. J. Environ. Anal. Chem.*, 2021, **101**, 506–512.
26 A. Popova, *Coke Chem.*, 2017, **60**, 361–365.
27 Z. Li, C. Lu, Z. Xia, Y. Zhou and Z. Luo, *Carbon*, 2007, **45**, 1686–1695.

28 Q. Guan, R. Su, M. Zhang, R. Zhang, W. Li, D. Wang, M. Xu, L. Fei and Q. Xu, *New J. Chem.*, 2019, **43**, 3050–3058.
29 S. Kalytchuk, L. Zdražil, M. Scheibe and R. Zbořil, *Nanoscale*, 2020, **12**, 8379–8384.
30 H. Liu, J. Yang, Z. Li, L. Xiao, A. A. Aryee, Y. Sun, R. Yang, H. Meng, L. Qu and Y. Lin, *Anal. Chem.*, 2019, **91**, 9259–9265.
31 S. Qu, D. Zhou, D. Li, W. Ji, P. Jing, D. Han, L. Liu, H. Zeng and D. Shen, *Adv. Mater.*, 2016, **28**, 3516–3521.
32 J. Wang, J. Wang, W. Xiao, Z. Geng, D. Tan, L. Wei, J. Li, L. Xue, X. Wang and J. Zhu, *Anal. Methods*, 2020, **12**, 3218–3224.
33 J. Bai, Y. Ma, G. Yuan, X. Chen, J. Mei, L. Zhang and L. Ren, *J. Mater. Chem. C*, 2019, **7**, 9709–9718.
34 L. Han, S. G. Liu, J. X. Dong, J. Y. Liang, L. J. Li, N. B. Li and H. Q. Luo, *J. Mater. Chem. C*, 2017, **5**, 10785–10793.
35 Z. Liu, X. Lu, M. Liu and W. Wang, *Molecules*, 2023, **28**, 2957.
36 S. Qu, X. Wang, Q. Lu, X. Liu and L. Wang, *Angew. Chem., Int. Ed.*, 2012, **51**, 12215–12218.
37 T. Zhang, J. Zhu, Y. Zhai, H. Wang, X. Bai, B. Dong, H. Wang and H. Song, *Nanoscale*, 2017, **9**, 13042–13051.
38 Y. M. Shirke, A. M. Abou-Elanwar, W.-K. Choi, H. Lee, S. U. Hong, H. K. Lee and J.-D. Jeon, *RSC Adv.*, 2019, **9**, 32121–33212.
39 M. A. Rauf, A. A. Soliman and M. Khattab, *Chem. Cent. J.*, 2008, **2**, 19.
40 P. Mohammad-Jafarieh, R. Salamat-Ahangari, M. Pourhassan-Moghaddam and A. Akbarzadeh, *J. Mol. Liq.*, 2021, **336**, 116360.
41 Y. Tu, Y. Yu, D. Xiao, J. Liu, Z. Zhao, Z. Liu, J. W. Lam and B. Z. Tang, *Adv. Sci.*, 2020, **7**, 2001845.
42 P. Hrdlovic, J. Donovalova, H. Stankovicova and A. Gaplovsky, *Molecules*, 2010, **15**, 8915–8932.
43 M. O. Alaş and R. Genç, *ACS Appl. Nano Mater.*, 2021, **4**, 7974–7987.
44 S. Mukherjee, E. Prasad and A. Chadha, *Phys. Chem. Chem. Phys.*, 2017, **19**, 7288–7296.
45 O. F. Mohamed, O.-H. Kwon, C. M. Othon and A. H. Zewail, *Angew. Chem., Int. Ed.*, 2009, **48**, 6251–6256.
46 F. Messina, M. Premont-Schwarz, O. Braem, D. Xiao, V. S. Batista, E. T. J. Nibbering and M. Chergui, *Angew. Chem., Int. Ed.*, 2013, **52**, 6871–6875.
47 Q. Fang, Y. Dong, Y. Chen, C.-H. Lu, Y. Chi, H.-H. Yang and T. Yu, *Carbon*, 2017, **118**, 319–326.
48 J. Yu, C. Liu, K. Yuan, Z. Lu, Y. Cheng, L. Li, X. Zhang, P. Jin, F. Meng and H. Liu, *Nanomaterials*, 2018, **8**, 233.
49 C. Reichardt, *Chem. Rev.*, 1994, **94**, 2319–2358.
50 R. Sato, Y. Iso and T. Isobe, *Langmuir*, 2019, **35**, 15257–15266.
51 A. Pramanik, S. Biswas and P. Kumbhakar, *Spectrochim. Acta, Part A*, 2018, **191**, 498–512.
52 D. Wang, P. Yang, Y. Hu, Z. Cui, Z. Du, P. Yang, S. Yi, J. Rao and Y. Zhang, *Powder Technol.*, 2023, **426**, 118670.
53 C. Zhang, D. Wang, L. Dong, K. Li, Y. Zhang, P. Yang, S. Yi, X. Dai, C. Yin and Z. Du, *Int. J. Mol. Sci.*, 2022, **23**, 9362.
54 Z. Du, D. Wang, X. Zhang, Z. Yi, J. Tang, P. Yang, R. Cai, S. Yi, J. Rao and Y. Zhang, *Int. J. Mol. Sci.*, 2022, **24**, 504.
55 D. Wang, Y. Hu, Z. Cui, P. Yang, Z. Du, Y. Hou, P. Yang, J. Rao, C. Wang and Y. Zhang, *J. Colloid Interface Sci.*, 2023, **646**, 991–1001.
56 G. E. Papanastasiou and I. I. Ziogas, *J. Chem. Eng. Data*, 1992, **37**, 167–172.
57 Y. Y. Liang, *Anal. Chem.*, 1990, **62**, 2504–2506.
58 F. Hou, X. Liu, X. Hao, G. Li, F. Lu and Q. Deng, *Dyes Pigm.*, 2021, **195**, 109667.
59 J. Wei, H. Li, Y. Yuan, C. Sun, D. Hao, G. Zheng and R. Wang, *RSC Adv.*, 2018, **8**, 37028–37034.